Acta metall. mater. Vol. 40, No. 7, pp. 1685–1690, 1992
Printed in Great Britain.

0956-7151/92 $5.00 + 0.00

MICROCRACKS TUNNELING IN BRITTLE MATRIX COMPOSITES DRIVEN BY THERMAL EXPANSION MISMATCH

S. HO and Z. SUO

Mechanical Engineering Department, University of California, Santa Barbara, CA 93106-5070, U.S.A.

(Received 4 November 1991)

Abstract—During processing, brittle composites are susceptible to cracks caused by residual stress. Matrix cracks parallel to fibers are considered in this paper. Each crack initiates from a porosity, confined by the neighboring fibers, tunneling in the matrix. The analysis uses the concept of steady-state tunneling, which eliminates several analytical artifacts in a previous calculation. The cracking coefficient is computed for the full range of elastic mismatch and several fiber arrangements, and is presented in a form that can be used in selecting viable constituents. Calculations also demonstrate that fiber–matrix interface plays a major role in cracking. A sliding interface relaxes tunnel edges, and thereby the energy release rate at the tunnel front.

Résumé—Pendant l'élaboration, des composites fragiles sont susceptibles de se fissurer par suite des contraintes résiduelles. On considère, dans cet article, des fissures de la matrice parallèles aux fibres. Chaque fissure commence sur une porosité, elle est confinée par les fibres avoisinantes et creuse un tunnel dans la matrice. Les analyses utilisent le concept de creusement de régime permanent qui élimine plusieurs artéfacts analytiques dans un calcul antérieur. Le coefficient de fissuration est calculé pour toute la gamme des désaccords élastiques et pour plusieurs arrangements des fibres; il est présenté sous une forme qui peut être utilisée pour sélectionner des constituants viables. Les calculs montrent aussi que l'interface fibre–matrice joue un rôle prépondérant dans la fissuration. Une interface glissante relâche les bords du tunnel, et par conséquent augmente la vitesse de libération de l'énergie sur le front du tunnel.

Zusammenfassung—Während der Verarbeitung neigen spröde Verbundwerkstoffe zu Rissen, die durch Restspannungen verursacht werden. In dieser Arbeit werden Matrixrisse parallel zu den Fasern betrachtet. Jeder Riß beginnt in einem porösen Bereich, der durch die benachbarten Fasern begrenzt wird und einen Tunnel in die Matrix bildet. Die Analyse beruht auf dem Konzept der stationären Tunnelbildung, wodurch verschiedene analytische Artefakte einer früheren Berechnung vermeiden werden. Der Rißbildungskeffizient wird für den gesamten Bereich der elastischen Fehlpassung und für verschiedene Faseranordnungen berechnet. Er wird in einer Form dargestellt, die die Auswahl geeigneter Konstituenten erleichtert. Eine gleitende Grenzfläche relaxiert Kanten des Tunnels und vergrößert damit die Energiefreisetzungsrate an der Tunnelfront.

1. INTRODUCTION

Ceramic and intermetallic matrix composites are fabricated at high temperatures ($\sim 1000°C$); huge residual stresses can be induced upon cooling. Matrix cracks (Fig. 1) form in systems like $MoSi_2$–SiC and $TiTaAl_2$–W, where the thermal expansion coefficient is larger in matrix than in fibers. Such cracking degrades materials and should be suppressed. In a recent study [1], it has been shown that a *cracking coefficient*, Ω, exists such that cracking is suppressed if

$$\Gamma_m/(R\epsilon_T^2\bar{E}_m) > \Omega. \tag{1}$$

The non-dimensional group consists of various design variables: R the fiber radius, Γ_m the matrix fracture energy, $\bar{E}_m = E_m/(1-\nu_m^2)$ where E_m and ν_m are Young's modulus and Poisson's ratio of the matrix, and ϵ_T the misfit strain defined by

$$\epsilon_T = \int_T^{T_0} \left(\alpha_m - \alpha_f\right) dT. \tag{2}$$

Here T_0 is the processing temperature, T the current temperature, and α the thermal expansion coefficient; subscripts m and f indicate matrix and fiber. Some preliminary results of Ω have been reported in [1].

Inequality (1) has been used in selecting constituents for viable composites [1]. An obvious possibility is matrix and fibers having similar thermal expansion coefficients, as exemplified by a γTiAl matrix reinforced by Al_2O_3 fibers. However, constituents selected for their superior chemical or mechanical performance may not have identical thermal expansion coefficients. Cracking can still be suppressed,

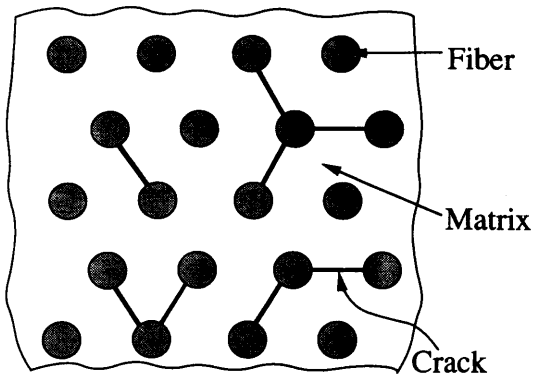

Fig. 1. Radial cracks caused by residual tensile stress in the matrix.

according to (1), by reducing the fiber radius. This concept has been demonstrated experimentally using $MoSi_2$–SiC composites with various fiber radii. The tensile residual stress in $MoSi_2$ matrix is huge (~ 2 GPa) and does *not* depend on fiber radius, but cracking is suppressed if SiC fibers are sufficiently thin ($R \sim 10\,\mu$m).

Previously calculated cracking coefficients agree qualitatively with experimental observations [1], but a few uncomfortable artifacts exist in the model. For example, the model assumes that a crack initiates from a through-thickness flaw [Fig. 2(a)], so that the relevant driving force is the energy release rate at the edge of the flaw, $\mathcal{G}$. However, $\mathcal{G} = \infty$ if the fiber is more compliant [2]. To avoid these, the analysis in the previous paper has been restricted to matrix and fibers having identical elastic constants, and the size of the initial flaw is arbitrarily assigned to be $R/2$.

A more realistic picture is suggested in Fig. 2(b). An initial flaw, roughly equiaxed and confined between two fibers, tunnels in the matrix. The relevant driving force is now the energy release rate at the curved front. Although a tunneling crack has a three dimensional geometry, the frontal energy release becomes insensitive to the tunnel length l after $l/a > 2$, and approaches a steady-state value [3, 4]

$$\mathcal{G}_{ss} = \frac{1}{2a}\int_0^a \delta(x)\sigma(x)\mathrm{d}x. \tag{3}$$

Here $\sigma(x)$ is the residual stress in the matrix prior to cracking, and $\delta(x)$ the opening profile of a through-thickness crack; each can be computed as a two-dimensional problem. Equation (3) is valid for any non-homogeneous material, so long as the material is homogeneous in the tunneling direction.

As such, the problem becomes well defined and the regular fracture mechanics can be applied. Dimensional considerations dictate that

$$\mathcal{G}_{ss} = \Omega \epsilon_T^2 \bar{E}_m R \tag{4}$$

with Ω being dimensionless and depending on such dimensionless variables as fiber volume fraction, fiber arrangement, and elastic mismatch. The tunnel cannot grow if

$$\mathcal{G}_{ss} < \Gamma_m. \tag{5}$$

Combination of (4) and (5) leads to criterion (1). Now the significance of fiber radius has a clear interpretation. The frontal energy release rate scales with the tunnel width, or the fiber separation, which in turn scales with fiber radius for a prescribed volume fraction.

The intent of this paper is to provide information on Ω over whole range of elastic mismatch and several important fiber arrangements. In following sections, $\delta(x)$ and $\sigma(x)$ are computed using finite elements, and $\mathcal{G}_{ss}$ is integrated according to (3). Both bonded and sliding interfaces are considered. A sliding interface accommodates large opening in the tunnel wake and, according to (3), give rise to high $\mathcal{G}_{ss}$.

2. A FIBER IN AN INFINITE MATRIX

Consider a long fiber in an infinite matrix (Fig. 3). Residual stress field prior to cracking can be determined analytically (Appendix A). The fiber is under uniform, triaxial compression. The matrix sustains a tensile hoop stress and a compressive radial stress, decaying with the distance away from the center of the fiber. A through-thickness crack under thermal loading is a generalized plane strain problem. The opening profile, $\delta(x)$, is computed by many runs of finite element analyses, with varying elastic mismatch and tunnel width. In the computation, Poisson's ratios are taken to be 1/3 for both matrix and fibers,

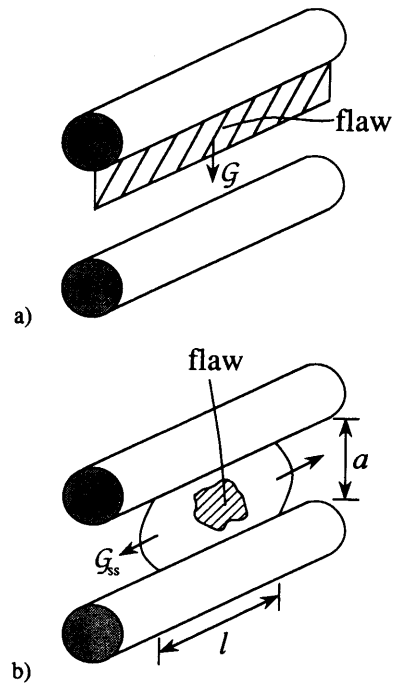

Fig. 2. (a) A through-thickness flaw grows to connect the fibers. (b) An initially equiaxed flaw tunnels between fibers.

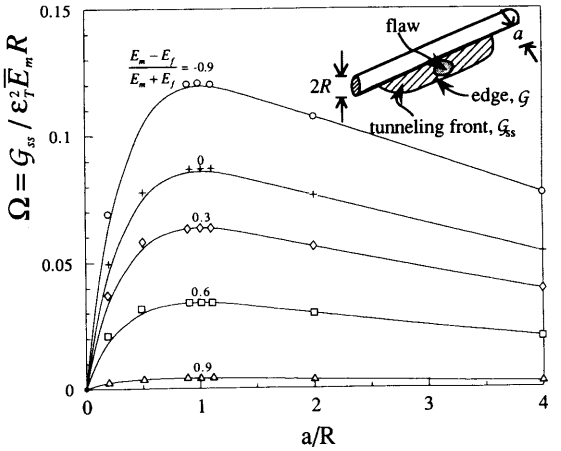

Fig. 3. The normalized energy release rate at the tunnel front.

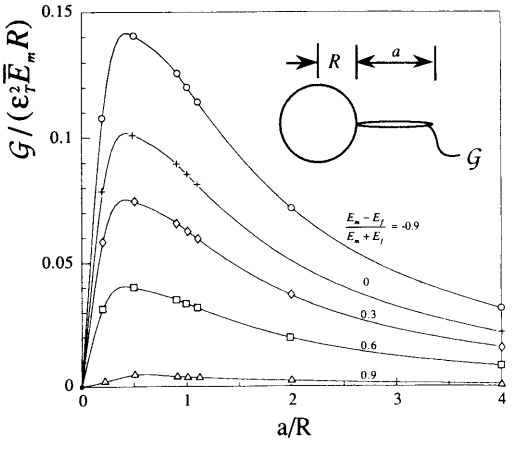

Fig. 5. Energy release rate at the edge of a through-thickness crack.

so that elastic mismatch can be specified by the ratio of Young's moduli, or more conveniently, by $(E_m - E_f)/(E_m + E_f)$.

Plotted in Fig. 3 is normalized $\mathcal{G}_{ss}$, or cracking coefficient Ω. The matrix provides constraint: the stiffer the matrix, the smaller the cracking coefficient. For a fixed elastic mismatch, Ω is small for both wide and narrow tunnels, attaining a maximum when $a \approx R$. This trend is anticipated: $\mathcal{G}_{ss}$ is small for a wide tunnel because the residual stress decays; $\mathcal{G}_{ss}$ is small for a narrow tunnel because the opening, δ, is limited.

Because the tunnel width, a, cannot be controlled in experiments, Fig. 3 is not useful unless a is determined. Around a thin, long fiber, equiaxed flaws are anticipated to be available at all sizes close to fiber radius and, upon cooling, the flaw subjected to the highest $\mathcal{G}_{ss}$ tunnels. Consequently, a can be selected to maximize Ω. Alternatively, the tunnel width can be determined such that the energy release rate is equal at the front and edge, i.e.

$$\mathcal{G} = \mathcal{G}_{ss}. \tag{6}$$

The two criteria are mathematically equivalent; a proof is given in the next paragraph. An inspection of Fig. 3 indicates that Ω attains maximum at $a/R \approx 1$ for any elastic mismatch. The value of Ω at $a/R = 1$ is therefore plotted in Fig. 4. The curve discriminates the dimensionless group, $\Gamma_m/(\varepsilon_T^2 \bar{E}_m R)$, into two regions: cracking is expected below the curve, but suppressed above.

We digress to the mathematical proof. As shown in [5], $\mathcal{G}_{ss}$ can be computed from

$$\mathcal{G}_{ss}(a) = \frac{1}{a} \int_0^a \mathcal{G}(a')\mathrm{d}a'. \tag{7}$$

$\mathcal{G}_{ss}$ is maximum if the derivative is zero, i.e.

$$\mathrm{d}\mathcal{G}_{ss}/\mathrm{d}a = (\mathcal{G} - \mathcal{G}_{ss})/a = 0. \tag{8}$$

That is, the tunnel width a that satisfies equation (6) also maximizes $\mathcal{G}_{ss}$. Incidentally, equation (7) can be used to compute $\mathcal{G}_{ss}$, which is convenient for situations where $\mathcal{G}$ is available, as demonstrated in Appendix B. However, equation (3) is more efficient in finite element calculations, particularly for tunnels confined by neighboring fibers.

Upon cooling from the processing temperature, a tunnel (with $a \approx R$) forms at a critical temperature, which can be determined by the curve in Fig. 4. With further cooling, the through-thickness crack spreads laterally, driven by the energy release rate at the edge, $\mathcal{G}$ (Fig. 5). The tunnel width a at a prescribed, lower temperature corresponds to $\mathcal{G} = \Gamma_m$. As such, matrix fracture energy, Γ_m, can be determined by using Fig. 5, in conjunction with an independent measurement of the final tunnel width, a. This method is accurate because the crack is stable and $\mathcal{G}$ is insensitive to a when $a > R$.

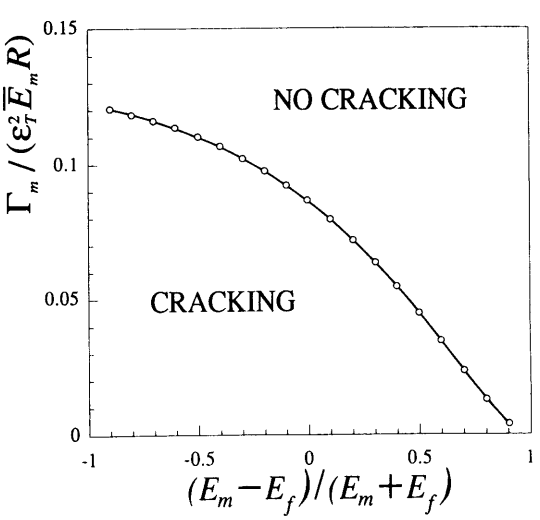

Fig. 4. The cracking coefficient for a fiber in an infinite matrix.

3. TWO OR MORE FIBERS

For two fibers in an infinite matrix (Fig. 6), both distributions needed to obtain $\mathcal{G}_{ss}$ from equation (3)—the residual stress prior to cracking, and the opening of a through-thickness crack—are obtained by analyzing the corresponding generalized plane strain problems using finite elements. The cracking coefficient Ω is plotted in Fig. 6, varying with elastic mismatch and fiber separation. Observe that both very closely and very widely spaced fibers give rise to low $\mathcal{G}_{ss}$, for similar reasons discussed in the previous section. A comparison of Figs 3 and 5 shows that Ω is smaller for an isolated fiber than for two fibers. This is anticipated since the residual stress is amplified by the presence of two fibers.

To explore the effect of volume fraction, calculations have been conducted for hexagonal fiber arrays (Fig. 7). The fiber volume fraction, f, and the separation, $2a$ are related by

$$f=\frac{\pi}{2\sqrt{3}}(1+a/R)^{-2} \tag{9}$$

The limiting volume fraction when fibers touch one another is $f\approx 0.91$. Tunnels are assumed to form between all the neighboring fibers, so that finite element analysis can be carried out for a periodic cell. The computed cracking coefficient Ω is plotted in Fig. 7.

The picture that cracks tunnel simultaneously between *all* the neighboring fibers is not realistic. Contrasted in Fig. 8 are values of Ω for the two extreme cases: one tunnel and a hexagonal array of tunnels. The former is obtained in Appendix B by analyzing one tunnel under the residual stress field of infinitely many fibers. In both cases fiber and matrix are assumed to have identical elastic constants. The cracking coefficient is much higher for a single tunnel than for the multiple tunnels. That is, upon cooling, a single tunnel forms at a certain temperature, followed by increasing number of tunnels at lower temperatures. Consequently, the curve for a single

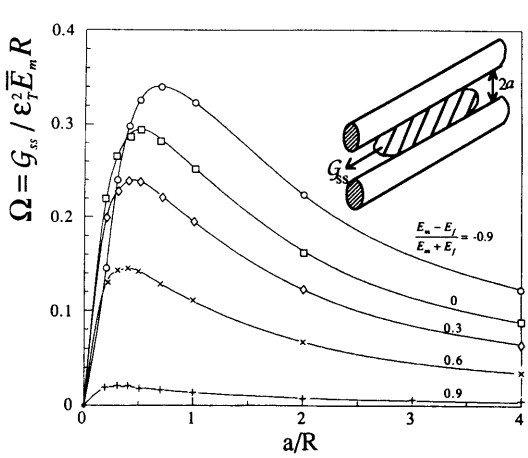

Fig. 6. A tunnel between two fibers in an infinite matrix.

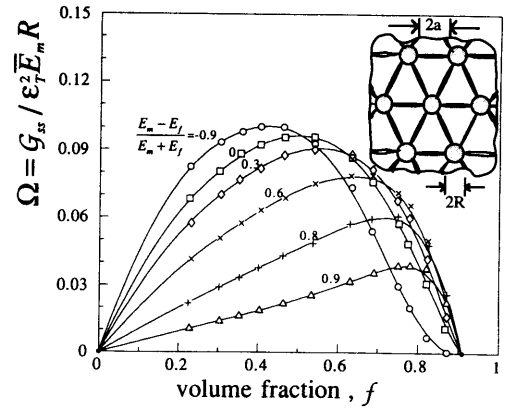

Fig. 7. Tunnels between a hexagonal array of fibers.

tunnel should be consulted in selecting constituents that completely suppress cracking.

Comparing Figs 6 and 8, one observes that Ω is smaller for many fibers than for two fibers. This is because fibers above and below a prospective crack plane contribute compressive stresses. It is also expected that because the residual stress in the matrix due to each fiber is localized around the fiber, the neighboring fibers, between which a crack tunnels, will make a dominant contribution to the frontal energy release rate. As such, the two-fiber solution can be used as a design criterion for multiple fibers irregularly distributed in a matrix.

4. EFFECTS OF INTERFACE SLIDING

To place the issue into perspective, the role of fiber–matrix interface on other properties of composites must be considered. When the fibers are used to enhance creep strength, good interface bonding is required. However, fibers used to enhance fracture toughness must debond and slide readily. In this case, the effect of interface debond on tunneling driving force must be included. In all the above computation, the matrix and fibers are assumed to be perfectly bonded, so that a tunnel edge is a sharp crack tip.

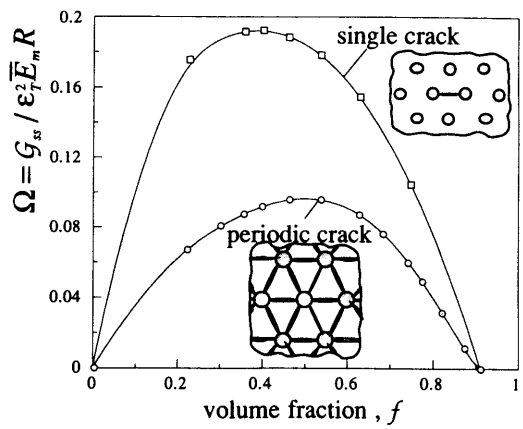

Fig. 8. Comparison between a single tunnel and many tunnels in the residual stress field due to a hexagonal array of fibers.

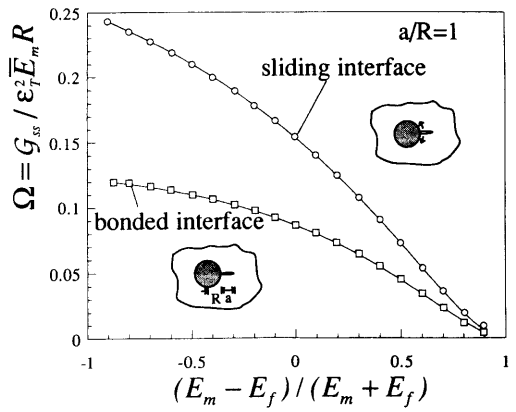

Fig. 9. Comparison between Ω-values for sliding and bonded interfaces (a single fiber).

A sliding interface will accommodate larger opening of the tunnel by relaxing the edges, and thereby provide larger driving force in accordance with (3). The following calculations are performed to provide the magnitude of the effects.

First consider a single fiber in an infinite matrix. Inserted in Fig. 9 are the tunnel wakes of the two situations: fully bonded and fully unbonded interface. The sliding stress is usually small compared to the residual stress and is therefore ignored. *The frictionless, fully debonded interface provides the upper bound of the effect of sliding.* Equation (3) is still valid; finite element calculations are carried out with contact, frictionless sliding interface, and the tunnel width is fixed at $a/R = 1$. As shown in Fig. 9, interface sliding increases Ω roughly by a factor of 2.

The effect is more pronounced for a tunnel between two fibers, since both edges are now relaxed. Finite element results are plotted in Fig. 10; both residual stress and crack opening are computed with contact, friction less sliding interface. As the fibers approach to each other, the residual stress prior to cracking is unbounded, and the opening of the tunnel wake is finite, so that $\mathcal{G}_{ss} \to \infty$ as $a \to 0$. The cracking

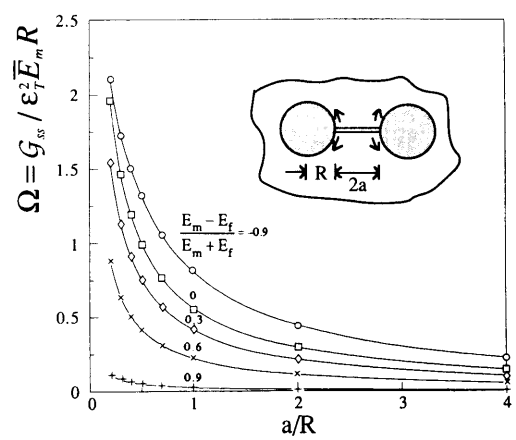

Fig. 10. Ω-values for a tunnel between two fibers with sliding interface.

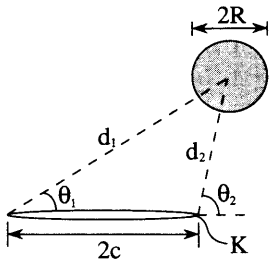

Fig. 11. A schematic of the kernel problem used to calculate stress intensity factors induced by many fibers.

coefficients in Fig. 10 may also be used to evaluate many fibers irregularly distributed in a matrix.

5. SUMMARY OF RESULTS

Matrix cracks parallel to fibers are modeled as steady-state tunnels. The incidence of cracking is governed by a dimensionless parameter (equation 1). The cracking coefficient, Ω, is computed for a fiber in an infinite matrix with bonded or sliding interfaces (Fig. 9). Similar results are given for a tunnel between two fibers (Figs 6 and 10). A sliding interface relaxes tunnel edges and thereby increases the driving force. Calculations of hexagonal fiber arrays reveal several important trends. A single tunnel sustains larger driving force than multiple tunnels (Fig. 8). Further, a comparison of Figs 6 and 8 shows that Ω for two fibers is larger than Ω for many fibers. As such, the two-fiber solutions, Fig. 6 and 10, provide a conservative design limit for composites with many fibers.

Acknowledgement—Support is provided by ONR-URI contract N0001486-0753, and by NSF grant MSS-9011571. Finite element code ABAQUS is used.

REFERENCES

1. T. C. Lu, J. Yang, Z. Suo, A. G. Evans, R. Hecht and R. Mehrabian, *Acta metall. matter.* **39,** 1883 (1991).
2. A. R. Zak and M. L. Williams, *J. appl. Mech.* **30,** 142 (1963).
3. Z. Suo, *Appl. Mech. Rev.* **43,** S276 (1990).
4. S. Ho and Z. Suo, to be published.
5. M. S. Hu, M. D. Thouless, A. G. Evans, *Acta metall.* **36,** 1301 (1988).
6. S. P. Timoshenko and J. N. Goodier, *Theory of Elasticity.* McGraw-Hill, New York (1970).
7. H. Tada, P. C. Paris and G. R. Irwin, *The Stress Analysis of Cracks Handbook.* Del Research, St. Louis, Miss. (1985).

APPENDIX A

Stress field can be determined analytically for a system consisting of a long fiber in an infinite matrix under thermal loading. Let (r, θ, z) be the cylindrical coordinates centered at the fiber. Upon cooling, an interface pressure, q, is developed, and the fiber is under a uniform, triaxial compression

$$\sigma_r^f = \sigma_\theta^f = -q, \quad \sigma_z^f = -\sigma. \tag{A1}$$

The matrix can be thought of as a hole subjected to an interior pressure q, and the stress field is [6]

$$\sigma_r^m = -q(R/r)^2, \quad \sigma_\theta^m = q(R/r)^2 \tag{A2}$$

Note that there is no σ_z component in the matrix when idealized to be infinite. The strains are caused by both stresses and thermal contraction in accordance with the generalized Hooke's law. Matching the fiber and matrix strains tangential to the interface, ϵ_z and ϵ_θ, one finds

$$\sigma = \epsilon_T E_f/(1 - kv_f), \quad q = k\sigma/2 \tag{A3}$$

with ϵ_T defined by equation (2), and the elastic mismatch parameter, k, given by

$$k = \frac{2E_m/(1+v_m)}{E_m/(1+v_m) + E_f/(1+v_f)}. \tag{A4}$$

The stress field is accurate except for a localized region around the fiber ends, as discussed in [1].

APPENDIX B

Analytic solutions of $\mathcal{G}_{ss}$ can be derived when matrix and fibers have identical elastic constants and when there is only one tunnel. These solutions are used to validate the finite element meshes for computing non-homogeneous composites.

Simplified from Appendix A for a fiber and a matrix having similar elastic constants, the stress field is

$$\sigma_r = -\tfrac{1}{2}\sigma(R/r)^2, \quad \sigma_\theta = \tfrac{1}{2}\sigma(R/r)^2 \tag{B1}$$

with

$$\sigma = \epsilon_T E/(1 - \nu). \tag{B2}$$

For a through-thickness crack of size $2c$ subjected to a non-uniformly distributed traction, $\sigma(x)$, and stress intensity factor is given by [7]

$$K = (\pi c)^{-1/2} \int_{-c}^{c} \left(\frac{c+x}{c-x}\right)^{1/2} \sigma(x)\mathrm{d}x. \tag{B3}$$

The stress in the present problem is due entirely to the residual stress prior to cracking. The integral can be evaluated analytically, giving

$$\frac{K}{\sigma\sqrt{R}} = \frac{1}{4}\left(\frac{\pi c}{R}\right)^{1/2}\left(\frac{d_1}{R}\right)^{-1/2}\left(\frac{d_2}{R}\right)^{-3/2} \cos\left(\frac{\theta_1}{2} + \frac{3\theta_2}{2}\right). \tag{B4}$$

Various quantities appeared in the equation are defined in Fig. 11. Energy release rate at the edge of the crack, $\mathcal{G}$, is related to K by the Irwin relation

$$\mathcal{G} = K^2/\bar{E}. \tag{B5}$$

The energy release rate at the curved tunnel front, $\mathcal{G}_{ss}$, can be evaluated using integral (7).

For a single fiber in an infinite matrix (Fig. 3) the results are

$$\frac{\bar{E}\mathcal{G}}{\sigma^2 R} = \frac{\pi}{8}(a/R)(1 + a/R)^{-3} \tag{B6}$$

and

$$\frac{\bar{E}\mathcal{G}_{ss}}{\sigma^2 R} = \frac{\pi}{16}(a/R)(1 + a/R)^{-2}. \tag{B7}$$

They are included in Fig. 5 and Fig. 3, respectively. Note that for this case $\mathcal{G}_{ss}$ attains the maximum at $a/R = 1$.

For two fibers in an infinite matrix (Fig. 6), K can be obtained by superimposing the contribution due to each fiber, and $\mathcal{G}_{ss}$ is found to be

$$\frac{\bar{E}\mathcal{G}_{ss}}{\sigma^2 R} = \frac{\pi}{4}\frac{\eta(\eta^2 + 4\eta + 2)}{(1+\eta)^2(1+2\eta)^2}, \quad \eta = a/R. \tag{B8}$$

This result is included in Fig. 6. Superposition is also applied to the hexagonal array of fibers which produces the curve in Fig. 8; a computer code is written to do the summation and integration.